NSP4 elicits age-dependent diarrhea and Ca^{2+}-mediated I^- influx into intestinal crypts of CF mice

ANDREW P. MORRIS,[1] JASON K. SCOTT,[1] JUDITH M. BALL,[2] CARL Q.-Y. ZENG,[2] WANDA K. O'NEAL,[3] AND MARY K. ESTES[2]

[1]*Departments of Integrative Biology and Internal Medicine-Gastroenterology, University of Texas at Houston Health Science Center, and* [2]*Divisions of Molecular Virology and Medicine-Gastroenterology and* [3]*Department of Molecular and Human Genetics, Baylor College of Medicine, Houston, Texas 77030*

Morris, Andrew P., Jason K. Scott, Judith M. Ball, Carl Q.-Y. Zeng, Wanda K. O'Neal, and Mary K. Estes. NSP4 elicits age-dependent diarrhea and Ca^{2+}-mediated I^- influx into intestinal crypts of CF mice. *Am. J. Physiol.* 277 (*Gastrointest. Liver Physiol.* 40): G431–G444, 1999.—Homologous disruption of the murine gene encoding the cystic fibrosis (CF) transmembrane conductance regulator (CFTR) leads to the loss of cAMP-mediated ion transport. Mice carrying this gene defect exhibit meconium ileus at birth and gastrointestinal plugging during the neonatal period, both contributing to high rates of mortality. We investigated whether infectious mammalian rotavirus, the recently characterized rotaviral enterotoxin protein NSP4, or its active $NSP4_{114–135}$ peptide, can overcome these gastrointestinal complications in CF ($CFTR^{m3Bay}$ null mutation) mice. All three agents elicited diarrhea when administered to wild-type ($CFTR^{+/+}$), heterozygous ($CFTR^{+/-}$), or homozygous ($CFTR^{-/-}$) 7- to 14-day-old mouse pups but were ineffective when given to older mice. The diarrheal response was accompanied by non-age-dependent intracellular Ca^{2+} mobilization within both small and large intestinal crypt epithelia. Significantly, NSP4 elicited cellular I^- influx into intestinal epithelial cells from all three genotypes, whereas both carbachol and the cAMP-mobilizing agonist forskolin failed to evoke influx in the $CFTR^{-/-}$ background. This unique plasma membrane halide permeability pathway was age dependent, being observed only in mouse pup crypts, and was abolished by either the removal of bath Ca^{2+} or the transport inhibitor DIDS. These findings indicate that NSP4 or its active peptide may induce diarrhea in neonatal mice through the activation of an age- and Ca^{2+}-dependent plasma membrane anion permeability distinct from CFTR. Furthermore, these results highlight the potential for developing synthetic analogs of $NSP4_{114–135}$ to counteract chronic constipation/obstructive bowel syndrome in CF patients.

cystic fibrosis transmembrane conductance regulator; halide permeability; NSP4 enterotoxin; rotavirus

THE MOST COMMONLY REPORTED gastrointestinal manifestation in cystic fibrosis (CF) is malabsorption due to pancreatic insufficiency, caused by occlusion of the pancreatic ducts by abnormally viscous mucus secretions. This alteration in intraluminal fluid and mucus content extends to other solid organs and hollow viscera of the gut, creating the clinical conditions of meconium ileus at birth and distal intestinal obstruction syndrome, chronic constipation with acquired megacolon, and rectal prolapse in older individuals (1).

Underlying these gastrointestinal complications is the basic defect in CF, which is caused by mutations in the gene that encodes the CF transmembrane conductance regulator (CFTR; Ref. 43). The most commonly reported mutation in CF, accounting for the genetic defect in 60–70% of the chromosomes of CF individuals, is a three-base-pair deletion that removes phenylalanine at position 508 (ΔF508) of the CFTR protein (54). CF patients homozygous for this mutation exhibit the severe clinical phenotype of lung disease, pancreatic insufficiency, and predisposition to gastrointestinal obstruction (48). Electrophysiological analysis of the gut mucosa isolated from these individuals demonstrates a lack of cAMP-dependent fluid secretion (6, 37, 53). Reduced fluid transport, which is the primary cellular defect of CF epithelia, is believed to significantly enhance the pathology of mucus plugging in the gut.

Over the past six years, mouse models for CF that duplicate the pathophysiological phenotype of CF in the human intestine have been produced with the use of gene-targeting techniques. Transgenic CFTR-deficient animals fail to exhibit CFTR-mediated fluid secretion and present with gastrointestinal disease (15). In this study, we utilized the $CFTR^{m3Bay}$ null mutation mouse as a model for CF to investigate whether infectious rotavirus or the novel rotaviral enterotoxin NSP4 (3) can cause diarrhea. These mice fail to express functional CFTR protein because of multiple stop codons engineered within exon 3 of the murine CFTR genome (23).

Rotaviruses are the leading cause of severe gastroenteritis in infants and young animals (25). We have recently shown that NSP4, a rotavirus nonstructural protein (16), can cause diarrhea in young mice (3). Furthermore, electrophysiological analyses of intact intestinal mucosa from mice revealed that NSP4 mobilizes Ca^{2+} to mimic the secretory effects of the cholinergic agonist carbachol (CCh) in potentiating cAMP-dependent fluid secretion (3). We therefore asked whether NSP4 could evoke a diarrheal response in CFTR-depleted mice that exhibit no functional cAMP-dependent secretory pathway. Here, we demonstrate that NSP4 injected intraperitoneally into CFTR-deficient ($CFTR^{-/-}$) mouse pups induces an age-dependent diarrhea. Hence, CFTR-mediated changes in intestinal fluid transport were not directly involved in NSP4-elicited diarrhea. However, NSP4 was found

The costs of publication of this article were defrayed in part by the payment of page charges. The article must therefore be hereby marked "*advertisement*" in accordance with 18 U.S.C. Section 1734 solely to indicate this fact.

to mobilize Ca^{2+} in the crypt epithelia of both small and large intestine from wild-type ($CFTR^{+/+}$) as well as $CFTR^{-/-}$ pup and adult mice. These ex vivo data correlated with our in vitro findings in human gastrointestinal cell lines, in which NSP4 was shown to mobilize intracellular Ca^{2+} concentration ($[Ca^{2+}]_i$) via phospholipase C (PLC) activation and inositol 1,4,5-trisphosphate (IP_3) production (13). To investigate in greater detail the relationship between NSP4-induced epithelial cell Ca^{2+} mobilization and our previously reported age-dependent effects of NSP4 on murine intestinal mucosa Cl^- secretory current generation (3), we measured plasma membrane halide permeability changes ex vivo within the epithelial cells of isolated distal colon crypts. We found that NSP4 elicited age-dependent I^- influx into mouse pup crypts, inhibited by either the removal of bath Ca^{2+} or the transport inhibitor DIDS. The fact that this Ca^{2+}-dependent plasma membrane halide permeability pathway was not CFTR may provide a possible explanation as to why $CFTR^{-/-}$ mouse pups exposed to NSP4 develop age-dependent diarrhea.

MATERIALS AND METHODS

Reagents. Fura 2-AM and 6-methyoxy-*N*-(3-sulfopropyl) quinolinum (SPQ) were purchased from Molecular Probes (Eugene, OR). All other reagents, including DIDS, were purchased from Sigma (St. Louis, MO). NSP4 protein was fast-performance liquid chromatography- and affinity-purified from Sf9 insect cells infected with a recombinant baculovirus pAC461-G10 expressing simian rotavirus gene 10 (encoding NSP4), as described previously (13). The $NSP4_{114–135}$ peptide was synthesized at the University of Pittsburgh protein core laboratory and characterized as previously described (3).

Experimentally induced rotaviral infection or administration of NSP4 protein and $NSP4_{114–135}$ peptide to mouse pups. The simian rotavirus strain SA11 clone 3 (18) was used to infect neonatal CD-1 or $CFTR^{-/-}$ (23) mouse pups between the ages of 6 and 8 days. The genotype of the $CFTR^{-/-}$ mice was determined by polyacrylamide gel analysis of PCR products generated from DNA extracted from the tails of 1- to 2-day-old mice with the use of primers, as described previously (23). Either 10 or 20 diarrheal dose 50 of SA11 was administered in 50 μl of medium 199 by intragastric gavage. Alternatively, purified NSP4 protein or $NSP4_{114–135}$ was administered to C57B $CFTR^{-/-}$/$CFTR^{+/+}$ or CD-1 $CFTR^{+/+}$ mouse pups in a final volume of 50 μl of PBS by intraperitoneal injection. The doses used were 0.5 nmol of NSP4 protein or 100 nmol of $NSP4_{114–135}$ peptide because these doses were shown to be effective at inducing diarrhea in CD-1 $CFTR^{+/+}$ mouse pups (3).

Diarrheal activity measurements. To determine the presence of diarrhea following protein or peptide treatment, each mouse pup was examined every 1–2 h for the first 8 h and at 24 h after inoculation by gently pressing the abdomen. After virus inoculation, mouse pups were monitored twice a day for 4 days. Diarrhea was noted and scored from 1 to 4, with a score of 1 reflecting loose yellow stool and a score of 4 indicating completely liquid stool. A score of 2 (mucous with liquid stool, some loose but solid stool) and above was considered diarrhea. The scoring was performed on coded animals by a single person.

Crypt isolation and dye loading. Epithelial crypts from $CFTR^{-/-}$ mice (aged 8–12 days) were isolated from 3-cm segments of the mid to distal small intestine, 6 cm proximal to Bauhin's valve, and from the distal colon. After euthanasia by an overdose of ether and cervical dislocation, the entire small intestine and colon from the mouse were removed and flushed with ice-cold physiological saline. Individual intestinal segments were then mounted onto Perspex paddles and were immersed in Ca^{2+}-free standard Krebs buffered saline (in mmol/l: 107 NaCl, 4.5 KCl, 0.2 NaH_2PO_4, 1.8 Na_2HPO_4, 10 glucose, and 10 EDTA), and continuously gassed with 5% CO_2-95% O_2 at 37°C for 10–20 min. The crypts were then separated from the overlying mucosa by mechanical vibration for 30 s into ice-cold KCl HEPES saline (in mmol/l: 100 potassium gluconate, 20 NaCl, 1.25 $CaCl_2$, 1 $MgCl_2$, 10 HEPES, 10 glucose, 5 sodium pyruvate, and 0.1% BSA, pH 7.4), resembling the intracellular medium. Suspended crypts were then deposited (1,200 rpm for 1 min) onto poly-L-lysine-coated microscope coverslips (0 oz) with the use of a Shandon Cytopsin cell preparation system (13). The coverslips with crypts were then attached with vacuum grease to the base of customized perfusion wells and loaded in the dark with either Ca^{2+}-sensing or Cl^--sensing dye.

Fura 2-AM loading. Isolated crypts were incubated with 10 μM fura 2-AM at room temperature for 15–20 min. The coverslips were then mounted on an inverted Nikon microscope and superfused with standard HEPES-buffered extracellular saline (in mmol/l: 140 NaCl, 4.7 KCl, 1.13 $MgCl_2$, 10 HEPES, 10 glucose, and 1 $CaCl_2$, pH 7.4) for 5 min before imaging.

SPQ loading. Isolated crypts were loaded with SPQ at room temperature by a 6-min exposure to hyposmotic (80 mosM Cl^- or NO_3^-) HEPES-buffered extracellular saline containing 5 mM SPQ. After loading, the crypts were allowed to recover in isosmotic (140 mosM Cl^- or NO_3^-) HEPES-buffered extracellular saline for 10–15 min. This period was used when performing anion channel inhibitor studies to preload the crypts so that the reported spectral interference of 0.5 mM DIDS with SPQ fluorescence was minimized (61). DIDS binds irreversibly to cellular membranes; therefore, crypts were loaded and the bathing saline was changed before experimentation. The solution temperature was maintained at 37°C throughout these studies by prewarming the extracellular solutions and by water-jacketing the oil-immersion lens of the inverted microscope.

NSP4/$NSP4_{114–135}$ addition to isolated crypts. Small (100 μl) volumes of either the NSP4 protein or $NSP4_{114–135}$ peptide were superfused onto the isolated crypts during regular bath flow by N_2 pressure injection with the use of a Picospritzer. Low-resistance glass pipettes were filled with either compound dissolved in HEPES-buffered extracellular saline, and the tip was maneuvered close to the isolated crypt. Peptide or protein was released directly into the vicinity of the crypt for 40 s before being washed away by the bath flow.

$[Ca^{2+}]_i$ imaging. All experiments were carried out with the aid of a high-resolution camera imaging system as described previously (13). In brief, light emitted from fura 2-loaded cells at 510 nm was captured by an intensified video camera after exposure to both 340- and 380-nm excitation light. The camera signal was then digitally encoded and processed with image analysis software (IMAGE1/FL, Universal Imaging, Media, PA). The background-subtracted images were ratioed on a pixel-by-pixel basis to yield a bitmap field. Calibration of the fura 2 dye fluorescence was carried out with the use of the ionophore ionomycin under Ca^{2+}-free and Ca^{2+}-saturating conditions as described previously, and the $[Ca^{2+}]_i$ was calculated according to the Grynkiewicz equation (21). The $[Ca^{2+}]_i$ values of individual field pixels obtained by this procedure were color coded and displayed on an RGB monitor before being stored on the hard disk. Six collection areas were

chosen along the longitudinal axis (base to neck) of the crypt for spatial and time-dependent analysis of $[Ca^{2+}]_i$. The averaged ratio signal obtained from each of the six areas was digitally saved as a log file. The collected values from the six areas imaged within a single experiment were averaged together to give an experimental observation of one ($n = 1$). Values obtained from similarly placed collection areas along the longitudinal axis of different crypts were also averaged to see if any spatial localization to the Ca^{2+} signal existed. All protocols were completed within 1 h after crypt isolation.

Intracellular I^- imaging. The same high-resolution camera imaging system described above was utilized for these studies. Excitation for SPQ fluorescence was provided by a barrier filter centered at 365 ± 10 nm, reflected into the microscope objective by a 400-nm dichroic mirror. A neutral density filter (1.5 OD) was included in the light path to minimize photobleaching. The fluorescence emission from the SPQ-loaded cells passed through a 450 ± 25-nm barrier filter before being detected by the intensifier/camera. Fluorescent images were acquired at 0.8-s intervals and averaged over eight frames to yield a 540 × 480 field of mean pixel intensities. Six collection areas were then chosen within the longitudinal axis (base to midregions) of the crypt for spatial and time-dependent analysis of cellular SPQ fluorescence. SPQ does not exhibit excitation or emission shifts on anion interaction. Thus ratiometric imaging is not possible, and dye fluorescence is affected by volume changes within the cell (58). Both cAMP- and Ca^{2+}-mobilizing agonists have been reported to induce shrinkage without compensatory volume recovery in the lower to midregion of rat distal colonic crypts over a 5- to 30-min time course (11). To determine the extent of this effect over the time period of SPQ quenching (1–3 min), colonic crypts isolated from the distal colon of the mouse were loaded with the AM form of calcein, a dye inert to Ca^{2+} and pH changes in cells within the physiological range (8, 9). Cell volume measured over the first 30 s of agonist addition to the bath did not change appreciably (<2%) within the lower/midcrypt region (data not shown). These regions were utilized for all studies. Furthermore, to minimize possible volume effects on dye fluorescence, we chose an experimental design in which SPQ fluorescence quench by halide influx was employed rather than dequenching following halide efflux. This ensured that agonist-induced cell shrinkage, if present, would act to decrease rather than to potentiate changes in plasma membrane halide permeability. Thus our reported values of SPQ quench may modestly underestimate agonist-evoked halide influx. The collected values from the six areas imaged within a single experiment were averaged together to give an experimental observation of one ($n = 1$).

Calculation of Stern-Volmer constants for halide quenching of SPQ. SPQ fluorescence is quenched collisionally by halide anions with different potency. Nonphysiological anions such as thiocyanate (SCN^-), Br^-, F^-, and I^- quench strongly in free solution with an efficacy greater than Cl^- ($Cl^- < Br^- < SCN^- < I^-$), whereas NO_3^- does not quench at all (27). The Stern-Volmer equation that describes this interaction is $F_o/F_{anion} = 1 + K_q[anion]$, where F_o is the fluorescence in the absence of anion, F_{anion} is the fluorescence in the presence of a given anion concentration, K_q (slope) is the Stern-Volmer quenching constant (in M^{-1}), and [anion] is the concentration of halide utilized (27). Stern-Volmer quenching constants for Cl^-, Br^-, and I^- anions were calculated from linear curves obtained over a concentration range of 0–150 mM halide (see RESULTS). The near-linear Stern-Volmer quench curve for I^- (Fig. 1) and the fact that plasma membrane I^- permeability changes occur largely through conductive pathways (see DISCUSSION and Refs. 36 and 63) led us to choose this anion to quantify agonist effects in isolated crypts.

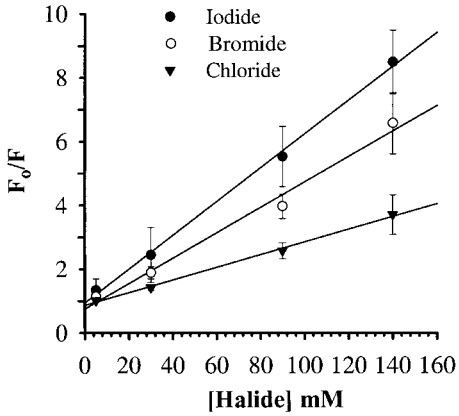

Fig. 1. Stern-Volmer plot for quenching of 6-methoxy-*N*-(3-sulfopropyl)quinolinum (SPQ) fluorescence by Cl^-, Br^-, and I^-. Isolated crypts from distal colon of wild-type cystic fibrosis transmembrane conductance regulator ($CFTR^{+/+}$) and heterogeneous ($CFTR^{+/-}$) mice were loaded with SPQ. Intracellular SPQ quench by different intracellular halide concentrations was induced with dual ionophore technique. F_o and F represent background and dye leak subtracted values of fluorescence in absence and in presence of quenching halide, respectively. Values are means ± SD.

To calibrate SPQ fluorescence in cells, the double ionophore technique, with the use of high-K^+ solutions containing nigericin (5 μM) and tributyltin (10 μM), was employed (7). In these experiments, isolated crypts were loaded with SPQ and hyposmotic NO_3^- (80 mM KNO_3) potassium saline and then were transferred to isosmotic NO_3^- (140 mM KNO_3) potassium saline containing the above ionophores. F_o/F_{anion} values were obtained by perfusing the crypts with varying concentrations of test halide (Cl^-, Br^-, or I^-) plus ionophore followed by SCN^- in the presence of valinomycin (5 μM) to completely quench the intracellular SPQ signal and obtain basal fluorescence values. Dye leakage was ~17% of the total cellular signal over 60 min (0.0125 ± 0.008 fluorescent units/s, $n = 60$). F_o and F_{anion} values were corrected for this signal on a per-experiment basis by interpolation from the fluorescence intensity, measured in cells bathed in Cl^--free medium at the onset of the experiment and at the end of the experiment or by back extrapolation from the rate of change measured during the SCN^- fluorescence minimal quench signal (i.e., $F_o - F_{ex}$ and $F_{anion} - F_{ex}$, where F_{ex} = background fluorescence at the time of measurement). Both methods gave comparable values. All experimental protocols were completed within 15–20 min. The Stern-Volmer quench constants for halide quenching of SPQ in pup and adult crypts (see RESULTS) were utilized to calculate the halide influx rates in the standard experimental procedure according to the following equation: $J_{I^-} = (F_o/K_q \cdot F^2) \cdot (\Delta F/\Delta t)$, in which $\Delta F/\Delta t$ is the rate of fluorescence change measured at *time 0*. In addition to this method, running averages of halide influx at 1.6-s intervals during the first 40 s of the fluorescence quench were calculated.

Standard experimental procedure for measuring agonist-stimulated I^- influx. SPQ-loaded crypts were perfused with HEPES-buffered $NaNO_3$ containing extracellular saline, and, after establishment of a stable fluorescence signal, bath NO_3^- was replaced with I^- (140 mosM). The quenched SPQ fluorescent signal (NO_3^- does not quench SPQ nor compete with I^-) was recorded over predefined measurement windows along the base to midcrypt axis. Basal rates of I^- influx (J_{I^-}) were then calculated with the use of the Stern-Volmer quench constants for I^- obtained for either mouse pup or adult crypts

(see *Calculation of Stern-Volmer constants for halide quenching of SPQ* and RESULTS). Cl^- was then reintroduced, and I^- was simultaneously removed from the bath. A single agonist was administered during this recovery phase (forskolin, FSK) or after establishment of a new stable fluorescence signal (CCh or NSP4) when bath I^- was reintroduced in Cl^--free saline. The resulting agonist-stimulated SPQ quench curve was recorded, and $J_{I^-agonist}$ was calculated. Agonist-induced changes in I^- influx rate were then calculated from pooled values of $J_{I^-agonist}$ and J_{I^-basal} as $\Delta J_{I^-} = (J_{I^-agonist} - J_{I^-basal})$. In addition to this approach, mean ± SD rates of fluorescence change at 1.6-s intervals over the first 40 s of fluorescence quench were graphically displayed in histogram format as change in agonist-induced quench rate, $\Delta R_{I^-} = (\Delta F/\Delta t_{agonist} - \Delta F/\Delta t_{basal})$. This later approach allowed us to determine latency and to record changes in dye quench unrelated to initial (*time 0*) changes in quench rate. All SPQ-loaded crypts were superfused with saline at the same bath perfusion rate (4 ml/min); solution exchange in the experimental chamber (200 μl) occurred within 3 s.

Statistical analysis. To determine statistical significance of differences between observations within an experiment, the paired Student's *t*-test was used. For statistical differences between experiments, the unpaired Student's *t*-test was used. Between 6 and 12 separate experimental observations pooled from different dye loadings were routinely collected for each experimental condition. The Fisher's exact test was used to estimate the probability of difference for diarrheal activity measurements within CF and non-CF groups in which the tabulated frequency of occurrence was too small for χ^2 analysis.

RESULTS

Effect of orally administered rotavirus and injected viral NSP4 peptide(s) in mouse pups. Inoculation of $CFTR^{-/-}$ mice with infectious SA11cl3 rotavirus caused diarrhea in four of five mice within 24–48 h (Table 1). When $CFTR^{+/+}$ or $CFTR^{+/-}$ mouse pups from the same C57B1/J6 background were infected with the SA11 virus, ~78% of the mice exhibited diarrhea (Table 1). Intraperitoneal injection of intact NSP4 protein or $NSP4_{114–135}$ was similarly found to elicit diarrhea in $CFTR^{+/+}$ or $CFTR^{+/-}$ mouse pups (66 and 70% responding, respectively). $CFTR^{-/-}$ mouse pups inoculated with these reagents exhibited diarrhea in 50% and 43% of these mice, respectively (Table 1). Diarrheal content was graded as equally severe as that encountered in $CFTR^{+/+}$ mice (3). Although the incidence of diarrhea caused by NSP4 protein or $NSP4_{114–135}$ appeared lower in the CF mouse studies, there was no significant difference between $CFTR^{+/+}$, $CFTR^{+/-}$, and $CFTR^{-/-}$ littermates (Fisher's exact test for 2 × 2 contingency tables; Ref. 32). All three reagents (SA11 virus, NSP4 protein, or $NSP4_{114–135}$) were effective diarrheal agents. In contrast, when infectious SA11cl3 virus was given to either adult $CFTR^{+/+}$, $CFTR^{+/-}$, or $CFTR^{-/-}$ mice, none exhibited diarrhea (Table 1).

Table 1. *Induction of diarrhea by rotavirus infection or NSP4 in $CFTR^{-/-}$ mice*

Inoculum	Dose	Route	Mouse Genotype: $CFTR^{+/+}$ or $CFTR^{+/-}$	Mouse Genotype: $CFTR^{-/-}$	P^{FET}
Mice 6–8 days old					
Rotavirus (SA11)	10–20 DD_{50}	Oral	7/9 (78%)	4/5 (80%)	>0.05
NSP4 protein	0.5–2 nmol	ip	8/12 (66%)	3/6 (50%)	>0.05
$NSP4_{114–135}$	100 nmol	ip	7/10 (70%)	3/7 (43%)	>0.05
Mice >21 days old					
Rotavirus (SA11)	10–20 DD_{50}	Oral	0/3 (0%)	0/5 (0%)	

Values are number of responders/total number of mice tested. Mice were genotyped after birth. NSP4 protein was expressed and purified as previously described (10). CFTR, cystic fibrosis transmembrane conductance regulator; DD_{50}, diarrhea dose 50; P^{FET}, Fisher's exact test.

NSP4 peptide mobilizes $[Ca^{2+}]_i$ levels in epithelial cells isolated from the small and large bowel of both $CFTR^{+/+}$ and $CFTR^{-/-}$ mice. Rotaviral protein production has been correlated with changes in $[Ca^{2+}]_i$ homeostasis (39) and with Ca^{2+}-dependent cytotoxicity during viral infection in cultured cells (33, 34). With the use of the human colonic epithelial cell line HT-29 clone 19A, which expresses plasmalemmal proteins found in both small and large intestinal cells, we recently demonstrated that exogenously added NSP4 and $NSP4_{114–135}$ peptide causes $[Ca^{2+}]_i$ mobilization by PLC-mediated IP_3 production (13). We therefore investigated whether the diarrheal effects of NSP4 and $NSP4_{114–135}$ peptide in vivo were also associated with native mucosal intestinal cell $[Ca^{2+}]_i$ mobilization. Fluorescence video microscopy was used to study the effects of exogenous NSP4 addition on $[Ca^{2+}]_i$ in intestinal crypts isolated from either small or large bowel of 8- to 13-day-old mouse pups.

Small intestinal crypts. Crypts from the small intestine were chosen in preference to villi, which dissociated during isolation. Addition of 100 nM NSP4 protein, a dose shown to promote near-maximal $[Ca^{2+}]_i$ rises in vitro (13), elicited rapid rises in $[Ca^{2+}]_i$ that lasted 2–5 min in $CFTR^{+/+}$, $CFTR^{+/-}$, and $CFTR^{-/-}$ small intestinal crypts. Resting $[Ca^{2+}]_i$ values of 126 ± 28 nM ($CFTR^{-/-}$, $n = 13$) and 110 ± 63 nM ($CFTR^{+/+}$ and $CFTR^{+/-}$, $n = 14$) increased to peak values of 205 ± 54 nM and 260 ± 116 nM, respectively (Table 2). A representative example (Fig. 2, *A–C*) shows consecutive images taken before, during, and after NSP4 addition to an epithelial crypt isolated from a $CFTR^{-/-}$ mouse. No significant difference was seen between mouse CFTR genotypes with respect to basal, peak, or net Ca^{2+} values ($P > 0.01$, Student's *t*-test; Table 2). These results indicated that NSP4 was an effective Ca^{2+}-mobilizing agonist in the small intestine and that Ca^{2+} homeostasis, both basal and agonist-stimulated, is unaffected by the CFTR gene knockout. Not all experimental crypts responded; 27 of 108 (25%) gave $[Ca^{2+}]_i$ rises. Increasing the dose of NSP4 from 100 to 500 nM and above did not increase the number of NSP4-responsive crypts (3 of 18 responded = 17%; data not shown).

Colonic crypts. When isolated crypts from the distal colon of $CFTR^{+/+}$, $CFTR^{+/-}$, and $CFTR^{-/-}$ mice were superfused with 100 nM NSP4 protein, $[Ca^{2+}]_i$ rises

Table 2. *Summary of the effects of 100 nM NSP4 and 100 μM CCh on $[Ca^{2+}]_i$ levels in either $CFTR^{-/-}$ or $CFTR^{+/+,+/-}$ small and large intestine mouse crypts*

		CCh				NSP4			
Tissue	Genotype	Basal $[Ca^{2+}]_i$	Peak $[Ca^{2+}]_i$	$\Delta[Ca^{2+}]_i$	*n*	Basal $[Ca^{2+}]_i$	Peak $[Ca^{2+}]_i$	$\Delta[Ca^{2+}]_i$	*n*
Colon	$CFTR^{-/-}$	98 ± 12	163 ± 16	65 ± 14*	6	113 ± 24	211 ± 64	97 ± 52	18
	$CFTR^{+/-,+/+}$	89 ± 46	335 ± 155	255 ± 155*	16	88 ± 35	242 ± 105	151 ± 84	36
Ileum	$CFTR^{-/-}$	142 ± 36	219 ± 55	77 ± 38	13	126 ± 28	205 ± 54	80 ± 37	13
	$CFTR^{+/-,+/+}$	95 ± 55	203 ± 104	106 ± 64	12	110 ± 63	260 ± 116	160 ± 93	14

Values are mean intracellular calcium concentration ($[Ca^{2+}]_i$) values (in nM) ± SD recorded from responding crypts. Experiments were performed on 8- to 13-day-old mice. Only 25% of crypt preparations responded. CCh, carbachol. *$P < 0.008$. All other comparisons between groups were not significant.

similar to those obtained from small intestinal crypts were recorded ($P > 0.1$, Student's *t*-test; Table 2). Peak NSP4-induced $[Ca^{2+}]_i$ values were similar in all three genetic backgrounds, although basal values were slightly, but not significantly, higher in $CFTR^{-/-}$ mice when all samples were pooled ($P > 0.01$, Student's *t*-test; Table 2). In our in vitro studies, we found that the NSP4-induced $[Ca^{2+}]_i$ mobilization was susceptible to predepletion by other agonists (remaining unresponsive for tens of minutes; Ref. 13). In contrast, NSP4-induced $[Ca^{2+}]_i$ release in both ex vivo colonic and ileal mucosal cell preparations was not desensitized by repetitive agonist administration ($n = 15$). In the $CFTR^{-/-}$ mouse crypt preparation shown in Fig. 3, identical $[Ca^{2+}]_i$ rises were seen for consecutive NSP4 or CCh followed by NSP4 challenge. Ca^{2+} homeostasis in the isolated crypt therefore appears to be more tightly regulated than in colonic cell lines.

To address why the NSP4 response rate of both small and large intestinal crypts was not >25%, we quantified the responsiveness of isolated crypts to the cholinergic agonist CCh. The addition of 100 μM CCh to the bath elicited $[Ca^{2+}]_i$ rises in a similar percentage of isolated crypts from both small and large intestine (33% responded; Table 2). Lower, more physiological doses of CCh would likely produce identical success rates for both agonists. These findings suggested that a more general cellular phenomenon, other than a lack of NSP4 receptors, was accountable for this effect. Because both M_3-muscarinic receptors and the cellular response to NSP4 have been shown to be sensitive to protease digestion (13), true in vivo NSP4 potency may have been masked.

Spatial analysis of the Ca^{2+}-mobilizing effects of NSP4 revealed no regional differences along the longitudinal axis of either colonic or small intestinal crypts. Mean resting values for base, mid, and neck regions (separated by ~25 μm) were 112 ± 142, 100 ± 25, and 102 ± 39 nM, rising to 250 ± 99, 229 ± 97, and 215 ± 79 nM, respectively ($n = 29$). The lack of localization-dependent effects on $[Ca^{2+}]_i$ indicates that, regardless of the cell maturity, the membranes of epithelial cells within the crypt remained responsive to NSP4. An example of this spatial homogeneity is shown in Fig. 4. In Fig. 4, a sustained component to NSP4-induced $[Ca^{2+}]_i$ mobilization is observed that disappeared on removal of NSP4 from the bath. Nominally Ca^{2+}-free conditions did not affect the Ca^{2+} response to NSP4 protein ($n = 12$, data not shown), confirming that the major source of the Ca^{2+} rise was from intracellular stores. However, under extracellular Ca^{2+}-free conditions, no sustained component was observed, indicating that Ca^{2+} influx also occurred. The effects of NSP4 ex vivo reproduced those recorded in vitro, which have been linked to the intracellular production of IP_3 (13).

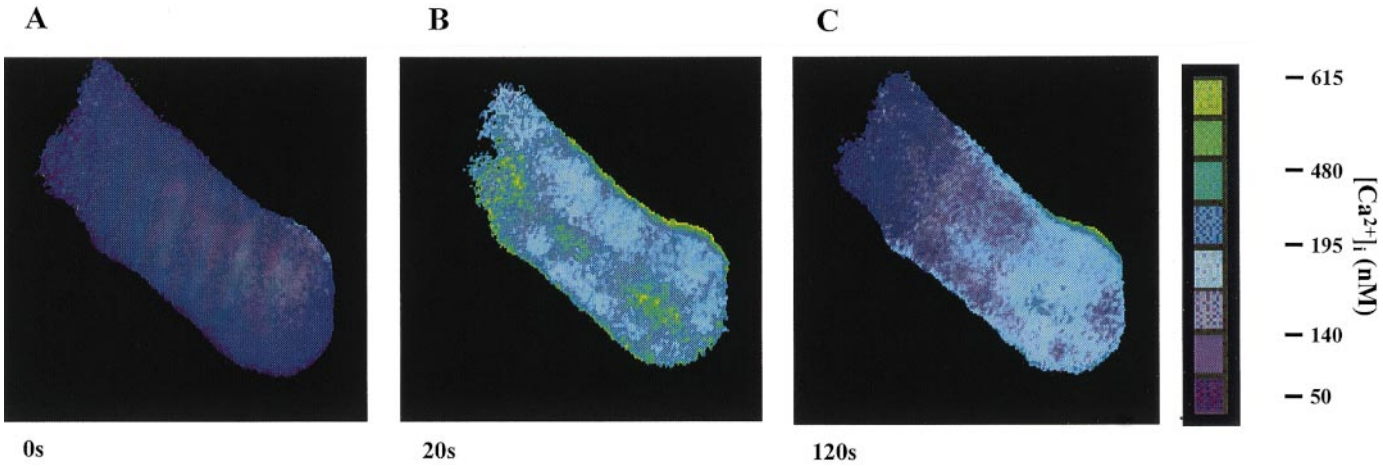

Fig. 2. Consecutive pseudocolor images of retroviral enterotoxin protein NSP4-induced intracellular Ca^{2+} concentration ($[Ca^{2+}]_i$) rise in an isolated CFTR-deficient ($CFTR^{-/-}$) small intestinal mouse crypt, loaded with fura 2. *A*: resting Ca^{2+} level of ~120 nM before agonist stimulation. *B*: peak Ca^{2+} level approaching 220 nM immediately after addition of 100 nM NSP4. *C*: gradual return of crypt to resting Ca^{2+} levels ~1.5 min after addition of NSP4.

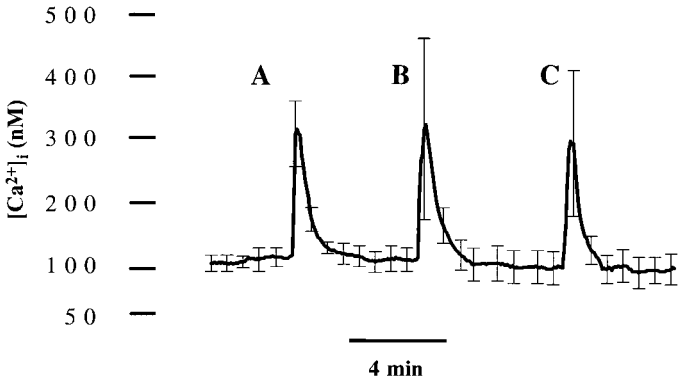

Fig. 3. A representative example of a single crypt. Average $[Ca^{2+}]_i$ values from 6 measurement areas along length of an isolated $CFTR^{-/-}$ colonic mouse crypt, showing effect of 100 nM NSP4 (*A*), 500 μM carbachol (CCh, *B*), and 100 nM NSP4 (*C*). SD values are shown as error bars.

NSP4 peptide mobilizes $[Ca^{2+}]_i$ levels in crypt epithelial cells from both pup and adult mice. Isolated colonic crypts from either normal ($CFTR^{+/+}$) C57B or BALB/c mice were loaded with fura 2 and exposed to 100 nM NSP4. In the example shown (BALB/c, Table 3), NSP4 mobilized Ca^{2+} in crypts from both 7- to 12-day- and >25-day-old mice. Although the mean number of BALB/c crypt responses was higher than that observed in the C57B background (data not shown), there was no age dependency to the magnitude of the NSP4-induced $[Ca^{2+}]_i$ rise (values were not statistically significant, unpaired *t*-test, $P > 0.05$, $n = 13$; Table 3). When CCh (100 μM) was applied after a NSP4-induced Ca^{2+} mobilization, 75% of pup crypts and 80% of adult crypts responded with a second $[Ca^{2+}]_i$ rise ($n = 13$). In this instance, the net agonist-induced $[Ca^{2+}]_i$ rise was significantly smaller in adult crypts ($P < 0.001$, unpaired *t*-test; Table 3). When CCh alone was applied to crypts, a similar age-dependent trend in Ca^{2+} mobilization was observed, which failed to be significant because of the great variability in the magnitude of the peak $[Ca^{2+}]_i$ values ($P > 0.05$; Table 3). These results indicated that events distal to NSP4-elicited $[Ca^{2+}]_i$ mobilization must regulate the age- and Ca^{2+}-dependent Cl^- secretory activity of NSP4 observed in the ex vivo mouse intestine (3).

Table 3. *Summary of the effects of 100 nM NSP4 and 100 μM CCh on $[Ca^{2+}]_i$ levels in pup and adult BALB/c mouse colonic crypts*

	$\Delta[Ca^{2+}]_i$, mM			
Agonist	BALB/c pup (7–12 days old)	*n*	BALB/c adult (>25 days old)	*n*
NSP4	112 ± 55	4	64 ± 36	9
NSP4 + CCh	502 ± 170*	4	102 ± 68*	9
CCh alone	323 ± 185	21	96 ± 99	40

Values are mean $[Ca^{2+}]_i$ values ± SD recorded from responding crypts. Number of crypts responding to NSP4 was similar in both pup (19%) and adult (22%) crypts. CCh was applied to NSP4-responding crypts. When CCh was applied alone to the bath, 40% of both pup and adult crypts responded. *$P > 0.001$, Student's unpaired *t*-test.

Calculation of Stern-Volmer constants for Cl^-, Br^-, and I^- in adult and pup mouse crypts. To separate carrier-mediated anion transport events from conductive anion transport in SPQ-loaded crypts, the halide I^- was used as a surrogate anion for Cl^-. I^- is not a substrate for either the Na^+-K^+-$2Cl^-$ cotransporter or Cl^-/HCO^- exchanger (36, 63). This choice was not, however, without technical drawbacks, because the Stern-Volmer relationships for Br^-, I^-, and SCN^- in free solution are reported to become positively nonlinear at >15 mM halide (24). Nonlinear increases in K_q above this concentration suggest that, in addition to

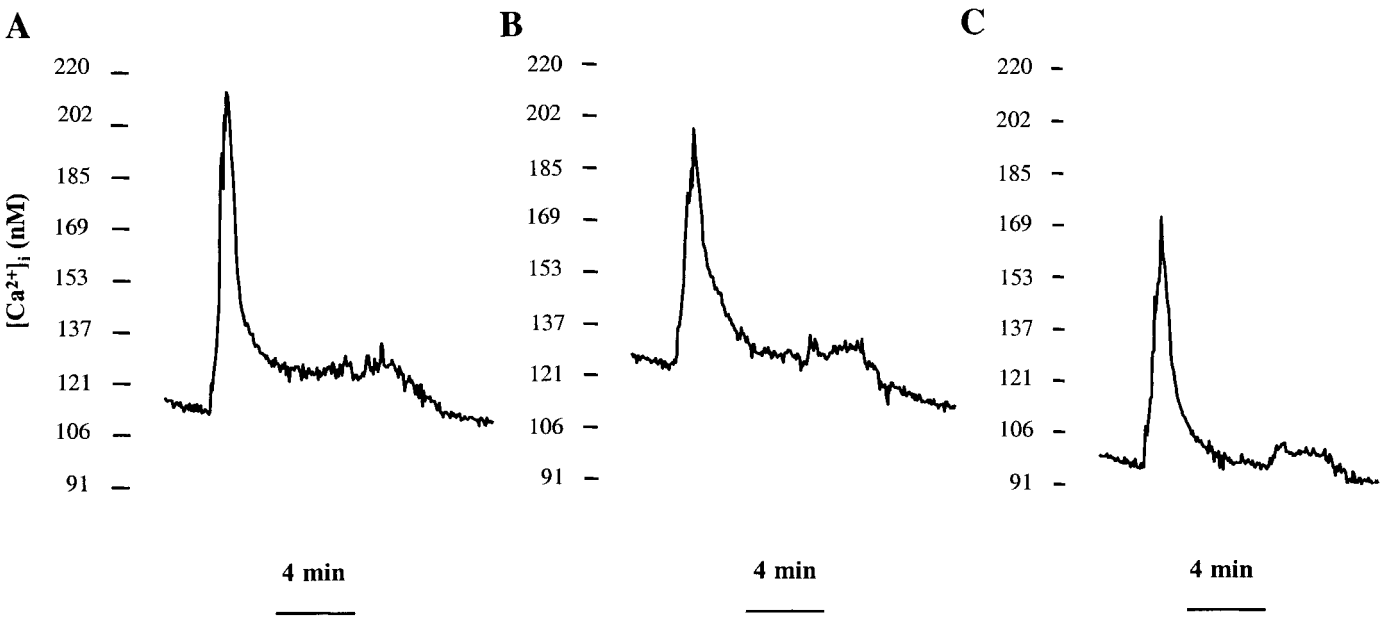

Fig. 4. $[Ca^{2+}]_i$ measurements taken from 3 different regions separated by ~15 μm along longitudinal axis of a $CFTR^{-/-}$ small intestinal crypt, showing magnitude of NSP4 $[Ca^{2+}]_i$ rise at crypt base (*A*), midregion of crypt (*B*), and near neck of crypt (*C*). Agonist (100 nM NSP4) was washed out of bath ~10 min after addition.

dynamic collision interactions, static interactions occur (i.e., those leading to nonfluorescent halide-SPQ complex formation; Ref. 28). Irrespective of the exact nature of this quenching (assumed to be static buffering), the dye would become noncalibrated at high halide concentrations, compromising I^- usefulness as a surrogate anion for conductive Cl^- influx. The Stern-Volmer relationship for Cl^- on the other hand has been demonstrated to remain linear when measured both in free solution and cells and shown to be the product of the dynamic collision-quench rate constant K_q (24). Stern-Volmer relationships for Cl^-, I^-, and Br^- were constructed in SPQ-loaded crypts with the use of the dual ionophore technique (Ref. 7; see MATERIALS AND METHODS). We found that apparent Stern-Volmer quench constants for both Br^- and I^-, calculated from halide concentrations of either <15 mM or <150 mM, exhibited modest <15% and slight <5% nonlinear increases in slope, respectively. This deviation was not large enough to accurately determine an additional buffering coefficient (28). Thus K_q values for Br^- and I^- were estimated by linear curve fitting and found to be 38.5 M^{-1} and 51.4 M^{-1}, respectively.[1] The K_q value for Cl^- was found to be 21.5 M^{-1} (measurements made in both pup and adult crypts, $n = 8$ per halide; Fig. 1), reflecting very well the ratio of SPQ collisional quench (1:1.7:1.9) reported for colonocytes (45). These values were slightly lower than those calculated in the rabbit crypts (45) and higher than those estimated in a variety of cancer cell lines (which range between 12 M^{-2} and 18 M^{-2} depending on cell type; Ref. 58). Because we failed to measure changes in tubular geometry (shrinkage) associated with agonist stimulation when confining our measurements to basal crypt areas, we did not resort to more theoretical measurements of the Stern-Volmer constant (22). With the use of these values, 50% of cellular SPQ quench would be achieved at 26, 19.6, and 47 mM Br^-, I^-, and Cl^-, respectively.

Calculation of basal and agonist-stimulated halide permeability. The dynamic K_q values determined above were used to calculate influx rates for the respective anions that were dependent on plasma membrane permeability and not on alterations in SPQ quench rate. Basal influx was in the order $I^- > Cl^- > Br^-$ (Table 4) for $CFTR^{+/+}$, $CFTR^{+/-}$, and $CFTR^{-/-}$ pup crypts. An age-dependent but not significant ($P > 0.05$) trend in basal influx was seen, with adult values being somewhat higher than those in pups. The lack of CFTR was associated with a statistically significant ($P < 0.001$) decrease in basal halide influx rate (J_{halide^-}) in $CFTR^{-/-}$ mice (Table 4).

[1] When utilizing I^- and NO_3^--containing saline, it could be argued that highly membrane-permeable oxidation species (e.g., IO_3^-, IO_5^-) may explain this additional buffering component. There is no clear way of establishing an equilibrium concentration of these anions in our solutions. However, this does not invalidate this well-established fluorescent procedure because matched controls are always performed (i.e., ± agonist) and increases in K_q would serve to underestimate influx.

Table 4. *Basal halide influx in CFTR-expressing ($CFTR^{+/+,+/-}$) and nonexpressing ($CFTR^{-/-}$) mouse pups*

Genotype	J_{I^-anion}, mM/s		
	Chloride	Bromide	Iodide
Pup $CFTR^{+/+,+/-}$	0.35 ± 0.05	0.33 ± 0.07	0.38 ± 0.1
Adult $CFTR^{+/+,+/-}$	0.37 ± 0.07	0.32 ± 0.07	0.45 ± 0.09
n	5	3	15
Pup $CFTR^{-/-}$	0.25 ± 0.08	0.24 ± 0.05	0.26 ± 0.07
Adult $CFTR^{-/-}$	ND	ND	ND
n	5	3	15

Values are means ± SD; *n*, number of animals. J_{I^-anion}, halide influx rate; ND, not detected. Rates were calculated in SPQ-loaded crypts using Stern-Volmer quench constants (K_q) derived in Fig. 1.

With the calculated K_q value for I^-, we tabulated changes in agonist-evoked I^- influx rate ($\Delta J_{I^-agonist}$) in response to FSK (10 μM), CCh (500 μM), and NSP4 peptide (500 nM) in all three CFTR genomic backgrounds (Table 5). Time-based histograms of changes in agonist-induced quench rate [$\Delta R_{I^-} = (\Delta F/\Delta t_{agonist} - \Delta F/\Delta t_{basal})$] are also shown (Figs. 5–7).

FSK-stimulated I^- influx into crypt cells was age independent and required CFTR. FSK, as predicted from previous studies (10, 45), induced significant I^- influx in both $CFTR^{+/+}$ and $CFTR^{+/-}$ mouse pup and adult crypts; $J_{I^-agonist}$ increased 3.7- to 4-fold over J_{I^-basal} and were statistically significant ($P < 0.001$, $n = 5$; Table 5). Age-dependent differences in the magnitude of ΔJ_{I^-} were absent ($P > 0.05$, $n = 5$; Table 5). Time-dependent analysis revealed that the peak FSK-induced quenching rate ($R_{I^-agonist}$) occurred 8–10 s after bath I^- exchange (Fig. 5*A*).

In contrast, when crypts isolated from $CFTR^{-/-}$ mouse pup littermates were exposed to FSK, much lower $J_{I^-agonist}$ and ΔJ_{I^-} values were obtained. In this instance, $J_{I^-agonist}$ failed to be significantly different from basal J_{I^-} values ($P > 0.05$) and both ΔJ_{I^-} and ΔR_{I^-} values were significantly lower than corresponding values obtained from $CFTR^{+/+}$ and $CFTR^{+/-}$ mouse pup crypts (ΔJ_{I^-} $CFTR^{-/-}$ = 0.03 ± 0.02 M^{-3}/s vs. ΔJ_{I^-} $CFTR^{+/+}$ and $CFTR^{+/-}$ = 1.4 ± 0.46 M^{-3}/s, $P < 0.001$, $n = 5$; Table 5 and Fig. 5*B*). The absence of CFTR was correlated with >95% inhibition of FSK-stimulated I^- influx into isolated mouse pup crypts. In all genotypes, FSK stimulated changes in influx in ~90% of crypts tested.

CCh-stimulated I^- influx into crypt cells was age independent and required CFTR expression. CCh (100 μM) $J_{I^-agonist}$ values were twofold greater than J_{I^-basal} values in wild-type and heterozygous CF genotypes and were significantly different ($P < 0.001$, $n = 5$; Table 5). The resulting ΔJ_{I^-} values from both groups displayed no age dependency (ΔJ_{I^-} pup = 0.62 ± 0.30 M^{-3}/s vs. ΔJ_{I^-} adult = 0.69 ± 0.24 M^{-3}/s, $n = 5$, $P > 0.05$; Table 5). These changes approximated to 51 and 40% of the values elicited by FSK in pup and adult crypts, respectively (Table 5). CCh-elicited ΔR_{I^-} changes were greatest 8–10 s after bath I^- exchange, with a latency

Table 5. *Summary of the effects of forskolin, CCh, and NSP4 on I^- influx rates in $CFTR^{+/+,+/-}$ and $CFTR^{-/-}$ mice*

Condition	$CFTR^{+/+,+/-}$					$CFTR^{-/-}$					
	J_{I^-basal}	$J_{I^-agonist}$	P	ΔJ_{I^-net}	n	J_{I^-basal}	$J_{I^-agonist}$	P	ΔJ_{I^-net}	n	P
FSK_{pup}	0.48 ± 0.1	1.9 ± 0.56	<0.001	1.4 ± 0.46	5	0.27 ± 0.14	0.3 ± 0.14	NS	0.03 ± 0.02	5	<0.001*
FSK_{adult}	0.43 ± 0.08	1.68 ± 0.5	<0.001	1.25 ± 0.29	5	ND	ND		ND		
P	NS	NS		NS							
CCh_{pup}	0.32 ± 0.08	0.94 ± 0.27	<0.001	0.62 ± 0.3	5	0.19 ± 0.06	0.3 ± 0.1	NS	0.11 ± 0.08	5	<0.001*
CCH_{adult}	0.53 ± 0.14	1.22 ± 0.32	<0.001	0.69 ± 0.24	5	ND	ND		ND		
P	NS	NS		NS							
$NSP4_{pup}$	0.4 ± 0.14	1.07 ± 0.32	<0.001	0.67 ± 0.24	5	0.22 ± 0.05	0.66 ± 0.13	<0.001	0.43 ± 0.1	5	NS*
$NSP4_{adult}$	0.6 ± 0.13	0.67 ± 0.14	NS	0.06 ± 0.02	5	ND	ND		ND		
P	NS	<0.001		<0.001							
$NSP4_{pup\text{-}EGTA}$	0.32 ± 0.08	0.3 ± 0.06	NS	−0.02 ± 0.06	4						
$NSP4_{pup\text{-}DIDS}$	0.29 ± 0.13	0.34 ± 0.14	NS	0.05 ± 0.06	4						

Values are means ± SD expressed as mM/s. FSK, forskolin; J_{I^-basal}, basal I^- influx rate; $J_{I^-agonist}$, agonist-stimulated I^- influx rate; ΔJ_{I^-net}, net agonist-stimulated I^- influx rate; ND, not determined; NS, not significant ($P > 0.05$). *P, unpaired Student's t-test of ΔJ_{I^-net} $CFTR^{+/+,+/-}$ vs. $CFTR^{-/-}$.

similar to that recorded for FSK (Fig. 6*A*). CCh was therefore a potent age-independent stimulator of plasma membrane I^- influx in CFTR-containing crypts, causing identical but smaller changes in I^- influx rate compared with FSK.

Like FSK, CCh failed to significantly increase the plasma membrane I^- influx rate in $CFTR^{-/-}$ mouse pup crypts. $J_{I^-agonist}$ and J_{I^-basal} values failed to be statistically different ($P < 0.05$, Student's t-test, $n = 5$; Table 5). The ΔJ_{I^-} recorded in CF mouse pup crypts was significantly smaller than $CFTR^{+/+}$ and $CFTR^{+/-}$ litter-

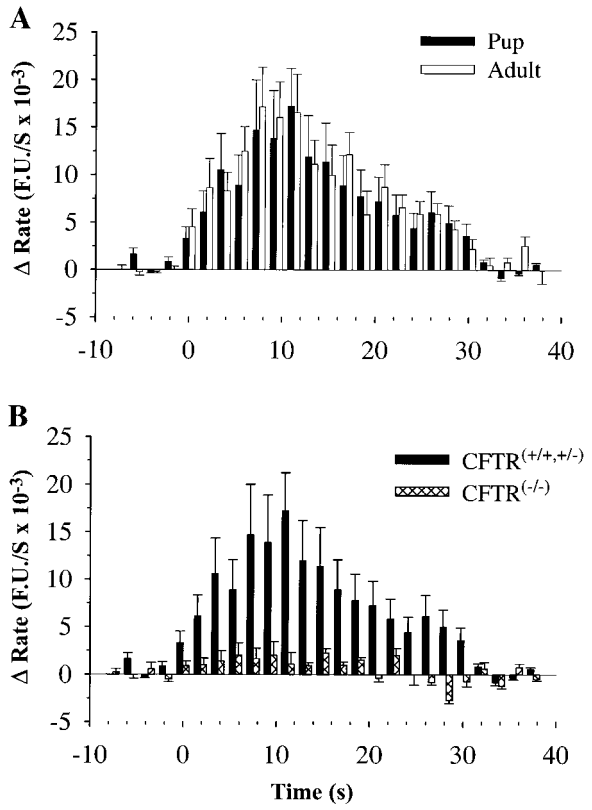

Fig. 5. Change in SPQ fluorescence quench rate in mouse distal colon crypts elicited by cAMP-mobilizing agonist forskolin (FSK, 10 μM). *A*: values obtained from adult and pup $CFTR^{+/+}$ and $CFTR^{+/-}$ mouse crypts, showing a lack of any age dependency. *B*: values obtained from pooled $CFTR^{+/+}$ and $CFTR^{+/-}$ and $CFTR^{-/-}$ pup crypts, demonstrating that effects of FSK on SPQ quench rate were dependent on CFTR expression. Values are means ± SD. FU, fluorescence unit.

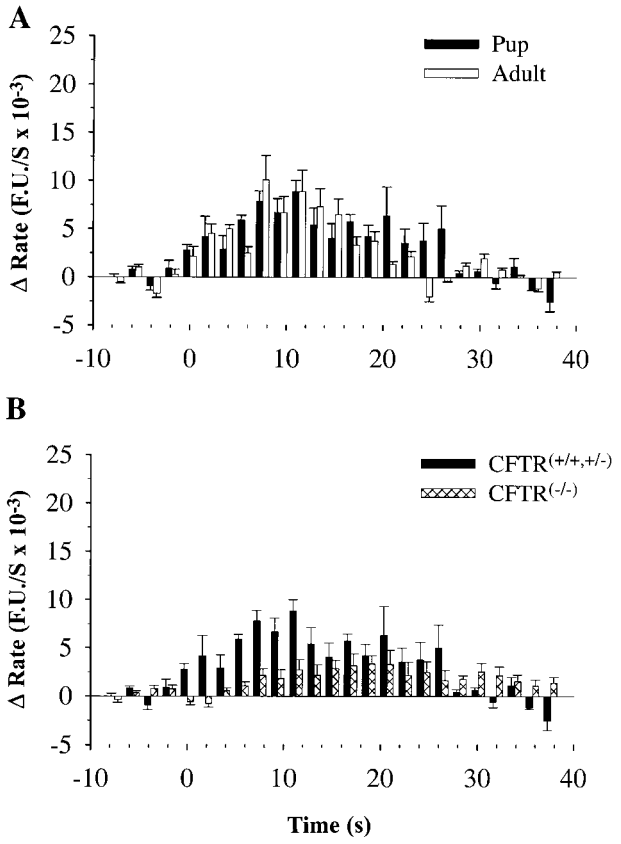

Fig. 6. Change in SPQ fluorescence quench rate in mouse distal colon crypts elicited by Ca^{2+}-mobilizing agonist CCh (100 μM). *A*: values obtained from pooled adult and pup $CFTR^{+/+}$ and $CFTR^{+/-}$ mouse crypts, showing a lack of any age dependency. *B*: values obtained from pooled $CFTR^{+/+}$ and $CFTR^{+/-}$ and $CFTR^{-/-}$ pup crypts, demonstrating that effects of CCh on SPQ quench rate were delayed and significantly smaller in magnitude when CFTR was absent from crypt. Values are means ± SD.

mate values ($CFTR^{-/-}$ $\Delta J_{I^-\,agonist} = 0.11 \pm 0.08$ M^{-3}/s vs. $CFTR^{+/+}$ and $CFTR^{+/-}$ $\Delta J_{I^-} = 0.62 \pm 0.3$ M^{-3}/s, $P < 0.001$, $n = 5$; Table 5). When ΔR_{I^-} for CCh was plotted by histogram analysis in the $CFTR^{-/-}$ background, quite different kinetics were observed. Both the onset and subsequent peak in ΔR_{I^-} trailed wild-type and heterozygous values by 4 and 18 s, respectively (Fig. 6*B*). This delay was not well defined by the single exponential fitted at *time 0* during initial rate analysis (J_{I^-}). Thus time-based histograms of rate change are shown. Peak values of CCh-induced ΔR_{I^-} recorded from $CFTR^{-/-}$ mouse pup crypts approximated to 60% of values recorded from wild-type and heterozygous genotypes. In all genotypes, CCh stimulated changes in ~65% of crypts tested. We therefore concluded that CCh, like FSK, requires CFTR to exert its major effects on plasma membrane I^- influx. Rate analysis revealed, however, that a slower component of SPQ quench rate was also present when CCh, but not FSK, was added to crypts from $CFTR^{-/-}$ pups.

NSP4-stimulated I^- influx into crypt cells was age dependent and largely independent of CFTR expression. NSP4 protein (100 nM) was found to elicit changes in plasma membrane I^- influx in crypts isolated from wild-type and heterozygous mouse CFTR genotypes. However, unlike either FSK or CCh, the effects of NSP4 were clearly age dependent (Table 5). In the pup crypt, NSP4 stimulated plasma membrane I^- influx by 2.7-fold, whereas, in the adult crypt, NSP4-stimulated I^- influx was <1.1-fold. Corresponding *P* values for $J_{I^-\,agonist}$ vs. J_{I^-basal} were significantly different for pup ($P < 0.001$) but not adult ($P > 0.05$) crypts. Net changes in NSP4-elicited influx rate were as follows: ΔJ_{I^-} pup = 0.67 ± 0.42 M^{-3}/s vs. ΔJ_{I^-} adult = 0.06 ± 0.02 M^{-3}/s, and were significantly different ($P < 0.001$, $n = 5$; Table 5). When the NSP4-induced change in I^- influx rate was displayed in histogram format, peak changes in influx rate had a lag of 10 s after introduction of I^- into the bath, similar to that recorded for both FSK and CCh (Fig. 7*A*).

Significantly, when NSP4 protein (100 nM) was tested on $CFTR^{-/-}$ mouse pup crypts, a threefold increase in I^- influx rate was recorded. $J_{I^-\,agonist}$ was statistically different from J_{I^-basal} ($P < 0.001$) and was not statistically different from $J_{I^-\,agonist}$ values obtained in wild-type and heterozygous CFTR backgrounds ($P > 0.05$; Table 5). The net change in NSP4-induced I^- influx rate approximated to 64% of $CFTR^{+/+}$ and $CFTR^{+/-}$ littermate values (ΔJ_{I^-} $CFTR^{-/-} = 0.43 \pm 0.1$ compared with ΔJ_{I^-} $CFTR^{+/+}$ and $CFTR^{+/-} = 0.67 \pm 0.42$). The ΔR_{I^-} values failed to exhibit either slow onset or delayed peak (as observed for CCh) in the $CFTR^{-/-}$ genotype (see above) but instead peaked 10 s after I^- introduction into the bath, paralleling NSP4, FSK, and CCh effects in CFTR-expressing crypts (Fig. 7*B*). In all genotypes, NSP4 stimulated changes in I^- influx in ~70% of crypts tested, a response rate twice that of NSP4-induced Ca^{2+} mobilization. Thus NSP4-evoked plasma membrane I^- influx was age dependent, occurring selectively in mouse pup crypts, and was

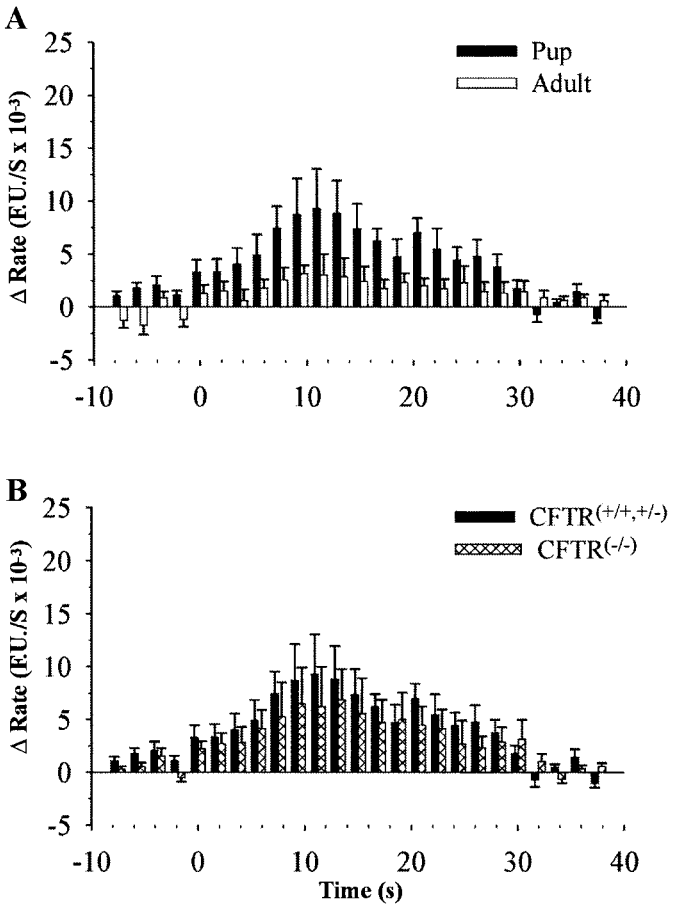

Fig. 7. Change in SPQ fluorescence quench rate in mouse distal colon crypts elicited by NSP4 (100 nM). *A*: values obtained form pooled adult and pup $CFTR^{+/+}$ and $CFTR^{+/-}$ mouse crypts, demonstrating that NSP4 effects were age dependent. *B*: values obtained from pooled $CFTR^{+/+}$ and $CFTR^{+/-}$ and $CFTR^{-/-}$ pup crypts, demonstrating that effects of NSP4 on SPQ quench rate were independent of CFTR expression. Values are means ± SD.

largely independent of CFTR expression. In crypts from wild-type and heterozygous CFTR pups, the NSP4-induced I^- influx rates were larger but not significantly different (1.56-fold, $n = 5$; Table 5). Thus CFTR expression may additionally be utilized by NSP4 to promote greater overall changes in plasma membrane halide permeability.

NSP4-induced I^- influx into pup crypt cells was dependent on $[Ca^{2+}]_i$ mobilization. To investigate the relationship between NSP4-induced Ca^{2+} mobilization and plasma membrane I^- influx, J_{I^-basal}, $J_{I^-\,agonist}$, and ΔJ_{I^-} were measured in $CFTR^{+/+}$ and $CFTR^{+/-}$ mouse pup crypts loaded and bathed in Ca^{2+}-free HEPES-buffered saline (nominally Ca^{2+}-free plus 1 mM EGTA). Basal I^- influx rate was not appreciably lower in this instance than in crypts bathed with standard (1 mM $CaCl_2$) extracellular saline (J_{I^-basal} Ca^{2+}-free = 0.32 ± 0.08 M^{-3}/s vs. J_{I^-basal} Ca^{2+}-containing = 0.4 ± 0.14 M^{-3}/s, values were not significantly different, $P > 0.05$, $n = 4$ and 15, respectively; Table 5). However, in all crypts the absence of bath Ca^{2+} completely inhibited NSP4-mediated I^- influx (ΔJ_{I^-} Ca^{2+}-free = -0.02 ± 0.06 M^{-3}/s vs. ΔJ_{I^-} Ca^{2+}-containing = 0.67 ± 0.42

M^{-3}/s, $P < 0.001$, $n = 4$ and 5, respectively; Table 5). These findings demonstrated that NSP4-stimulated plasma membrane I^- influx was dependent on $[Ca^{2+}]_i$ mobilization.

NSP4 protein-induced I^- influx in mouse pup crypt cells was inhibited by DIDS. The effectiveness of NSP4, but not CCh, at eliciting significant I^- influx into SPQ-loaded $CFTR^{-/-}$ mouse pups raised the question as to the nature of this novel conductive pathway. To begin to characterize this pathway, crypts were preexposed to 0.5 mM DIDS and then washed before experimentation. DIDS inhibits a variety of Cl^- channels identified in epithelial cells, including the outward-rectifying Cl^- channel, the swelling-activated Cl^- conductance channel, and the Ca^{2+}-sensitive Cl^- channel, but does not affect cAMP-stimulated CFTR Cl^- channels (reviewed in Ref. 19). DIDS also inhibits a variety of organic osmoltye exchange mechanisms (52) and the Cl^-/HCO_3^- exchanger (63). Basal I^- influx rate in the presence of DIDS was lower than controls but was not significantly different (J_{I^-basal} DIDS $= 0.29 \pm 0.13$ M^{-3}/s vs. J_{I^-basal} control $= 0.4 \pm 0.14$ M^{-3}/s, $P > 0.05$, $n = 5$; Table 5). This general halide transport inhibitor completely abolished the NSP4-elicited increase in plasma membrane I^- influx in all crypts ($J_{I^-agonist}$ DIDS $= 0.34 \pm 0.14$ M^{-3}/s vs. $J_{I^-agonist}$ control $= 01.07 \pm 0.32$ M^{-3}/s, $P < 0.001$, $n = 4$), and the net change in I^- influx rate reflected this difference (ΔJ_{I^-} DIDS $= 0.05 \pm 0.06$ vs. ΔJ_{I^-} control $= 0.67 \pm 0.24$, $P < 0.001$, $n = 4$; Table 5). Thus the ontogenically regulated NSP4-activated plasma membrane I^- influx pathway present in mouse pup crypts was DIDS sensitive.

DISCUSSION

Relationship between the diarrhea effects of infectious rotavirus and NSP4. The induction of diarrhea by NSP4 protein and $NSP4_{114–135}$ peptide compared with active rotavirus indicates that the enterotoxic effects of NSP4 may account for the initial diarrheal phase of rotaviral infection (3). During this period, diarrhea occurs without significant ultrastructural damage to the small intestinal mucosa (38, 57). This contrasts with diarrhea seen during the later stages of rotaviral infection in some animal species, in which villus blunting has been suggested to contribute to diarrhea by reducing small intestinal absorptive area (5). This later histopathological feature of rotaviral infection is not seen in all animal models; in the mouse, significant villus blunting is rare (38, 49). Therefore, loss of absorptive area is likely to be auxiliary to the underlying pathophysiological basis of diarrhea in this model. Supporting this hypothesis, we have shown that NSP4 and its active $NSP4_{114–135}$ peptide fail to cause significant histological damage to the mucosa when injected intraluminally or interperitoneally into wild-type mice (unpublished observations and Ref. 3).

Correlation between $[Ca^{2+}]_i$ mobilization and fluid transport in the gut. Addition of Ca^{2+}-mobilizing agonists such as CCh to intestinal mucosal sheets from either $CFTR^{-/-}$ mice or CF patients fails to evoke a Cl^- secretory current (6, 37, 53). This lack of response suggests that the cellular effects of Ca^{2+} mobilization on the Cl^- secretory current in the gastrointestinal tract occur secondary to cAMP-dependent activation of CFTR channels and are limited to the upregulation of basolateral membrane ion transporters and K^+ channels (51, 60). Results from NSP4-induced $[Ca^{2+}]_i$ mobilization in both native small and large intestinal crypts (Fig. 2, *A–C*, Fig. 3, and Table 2) support the hypothesis that the enterotoxic activity of NSP4 in normal mucosa may be partly due to the secondary effects of increased cellular Cl^- uptake at the basolateral plasma membrane and cellular hyperpolarization. These facilitating but not controlling mechanisms for intracellular Cl^- conduction across the luminal membrane do not explain all of our observations. Two important questions relating to the role of NSP4-induced $[Ca^{2+}]_i$ mobilization, namely the age-dependent effects of NSP4 on Cl^- secretion and diarrhea and the diarrheal effects of NSP4 in CF mice, remained unanswered.

NSP4-Ca^{2+} signaling does not directly regulate age-dependent Cl^- secretion. If changes in $[Ca^{2+}]_i$ levels alone were solely responsible for Cl^- secretion and diarrhea in mouse pups, then Ca^{2+} mobilization by NSP4 would be expected to be cell differentiation and/or crypt age dependent. Our studies found, however, that NSP4 mobilized $[Ca^{2+}]_i$ equally well in all crypt regions and was therefore independent of cellular maturity (Fig. 4). These findings contrast with the reported effects of both purinergic and muscarinic agonists on $[Ca^{2+}]_i$ in intestinal crypts, which show greater responsiveness in the basal region, where Cl^- secretion is believed to occur (29, 47). The more widespread $[Ca^{2+}]_i$ mobilization elicited by NSP4 would argue that antiabsorptive as well as prosecretory effects may be present in rotaviral-infected intestinal mucosa (see *An antiabsorptive model for NSP4-induced $[Ca^{2+}]_i$ mobilization*). Furthermore, the effects of NSP4 on $[Ca^{2+}]_i$ mobilization were neither strain dependent nor related to the age of the animals from which the crypts were isolated (Table 3). These findings therefore indicated that NSP4-mediated Ca^{2+} mobilization cannot directly account for the age dependency to Cl^- secretion and therefore secretory diarrhea reported by us in neonatal mice (3).

NSP4-Ca^{2+} signaling activates an age-dependent anion permeability in normal and CF mice. Both CCh and NSP4 have been shown to utilize PLC-dependent IP_3 signaling to elevate $[Ca^{2+}]_i$ (13). We therefore examined how NSP4, but not CCh, induces diarrhea in CF mouse pups. The SPQ fluorescence imaging technique has been used previously to measure basal and agonist-stimulated Cl^- permeability changes in both freshly isolated crypts (22) and primary cultures of rabbit (10, 45, 46) and human (45) distal colon. Cl^- transport measurements made with SPQ have demonstrated the absence of CFTR from epithelial cells of CF patients (41, 42, 50), and modeling studies have shown that the SPQ technique provides equivalent information to that obtained from either electrophysiological or isotopic flux studies (59).

Whereas both FSK and CCh elicited age-independent increases in I^- influx that are dependent on the

presence of CFTR (Table 5, Fig. 5, and Fig. 6, *A* and *B*), the effects of NSP4 were age dependent and largely CFTR independent (Table 5). Both CCh and NSP4 protein were more effective at causing plasma membrane permeability changes than causing generalized $[Ca^{2+}]_i$ mobilization. We believe this reflects both our technical limitations at isolating crypts with endogenous levels of receptor activity (see RESULTS) and the fact that Ca^{2+}-mobilizing agonists can couple efficiently with plasma membrane anion channels through localized $[Ca^{2+}]_i$ rises at the level of the plasma membrane that often do not provoke a generalized $[Ca^{2+}]_i$ mobilization (35).

The lack of an age dependency for CFTR-dependent I^- permeability changes corroborated Cl^- transport studies made in weaning and adult rat and pig colon but differed from the age-dependent effects of cGMP or *Escherichia coli* heat-stable enterotoxin (STa) in primary cultures of weaning and adult rabbit colon. In these instances agonist responses were greater in crypts isolated from older mice (10). Differences may, however, reflect the fact that Cl^- was used as a quencher in the latter studies, and rates may represent both conductive and nonconductive components of plasma membrane Cl^- permeability. In addition, STa effects on transmucosal Cl^- secretion and crypt Cl^- permeability are absent in the CF mice (20). Thus NSP4 utilizes a different plasma membrane permeability pathway in distal colon crypts from that utilized by STa or its mammalian counterparts, guanylin or uroguanylin, and other nitroso compounds of nitric oxide-signaling pathways.

The age dependency to NSP4-elicited changes in plasma membrane I^- influx suggests that NSP4-elicited diarrhea in CF mouse pups (Table 1) may be brought about by the activation of a novel cellular permeability pathway. The fact that neither FSK nor CCh promoted similar changes in CF mice, and that NSP4-induced I^- permeation was both Ca^{2+} dependent and blocked by DIDS (Table 5), supported the hypothesis that we are reporting on a different permeability pathway. NSP4-induced I^- influx into $CFTR^{-/-}$ mouse pup crypts was ~60% of that elicited in the wild-type and heterozygous background. This difference may possibly explain the higher, but not significantly different, incidence of diarrhea reported for infectious rotavirus, NSP4 protein, and $NSP4_{114-135}$ peptide in $CFTR^{+/+}$ and $CFTR^{+/-}$ mice. NSP4-induced $[Ca^{2+}]_i$ mobilization would be expected to facilitate both CFTR-dependent and CFTR-independent anion permeation by upregulating Ca^{2+}-dependent secondary active transport mechanisms at the basolateral membrane.

Our findings would also provide a functional explanation for the recent observations of Angel and colleagues (2), who demonstrated that CF mice and their non-CF siblings exhibit diarrhea after rotaviral infection. The age- and Ca^{2+}-dependent changes in intestinal epithelial cell plasma membrane anion permeability evoked by NSP4, shown in this study to be CFTR independent, may contribute to (or constitute) the acute phase of the rotaviral diarrheal response. This cellular phenomena would precede immune/morphological changes occurring within the mucosa after viral infection.

Candidate anion conductances for NSP4-induced age-dependent permeability changes in the mouse pup crypt. Although the plasma membrane halide permeability changes promoted by NSP4 were clearly Ca^{2+} dependent and could be inhibited pharmacologically, our investigations have yet to confirm the biophysical nature of the conductance. Furthermore, the SPQ technique does not allow us to determine the plasma membrane location of the NSP4-elicited I^- influx. Future studies utilizing alternate methods should address these questions. Even so, at this point, it is of interest to consider candidate conductances that may participate in this phenomena.

Direct activation of apical plasma membrane Ca^{2+}-sensitive Cl^- channels by classical PLC-dependent Ca^{2+}-mobilizing secretagogues, although clearly demonstrated in gastrointestinal cell lines and epithelial cells from other organs, e.g., the lungs (19), has not been shown in native intestinal epithelia. However, both enteroendocrine and macrophage/lymphocyte populations of the gut are known to secrete cryptdin proteins, some of which are believed to act themselves as anion conductances (30), whereas others, notably the defensins, are proposed to act at nanomolar concentrations to stimulate Ca^{2+}-dependent Cl^- secretion (4, 31). We therefore propose that NSP4 either *1*) itself creates a conductance in the apical plasma membrane, *2*) activates a dormant Ca^{2+}-activated anion channel within this membrane with biophysical properties similar to those recorded in vitro (reviewed in Ref. 19) through its stimulatory effects on PLC-induced $[Ca^{2+}]_i$ mobilization (13), or *3*) acts as a regulatory protein at the level of Ca^{2+}- or anion-channel signaling to elicit Ca^{2+}-dependent permeability changes across the cellular plasma membrane. CCh failed to promote similar changes in the initial rate of I^- influx into CF mouse pup crypts as NSP4 but elicited a response with a delayed onset, consisting of ~20% of wild-type and heterozygous CFTR values (Table 5 and Fig. 6*B*). Because supramaximal concentrations of CCh were used, these differences do not reflect dose dependency and argue against the presence of an ontogenically regulated conductance that can be stimulated by all Ca^{2+}-mobilizing agonists. The delayed onset changes in I^- permeability promoted by CCh (Fig. 6*B*) are unlikely to be localized to the apical membrane because it is clear that CCh fails to elicit a Cl^- secretory response in CF mucosal sheets (6, 37, 53).

A possibility exists that NSP4 may activate a native cell counterpart of osmotically regulated Cl^- channels. These conductances, although not directly activated by Ca^{2+}, are indirectly Ca^{2+} sensitive and have been shown to participate in regulatory volume decreases (RVD) in intestinal epithelia (12). These channels, believed to be localized on the basolateral plasma, participate in the maintenance of fluid and osmolyte absorption. They are functionally expressed in the surface and neck regions of the crypt as well as the small intestinal villi, areas known to exhibit RVD (11)

and have been shown to be impaired in $CFTR^{-/-}$ mice (55). Our SPQ fluorescent measurements were made, however, in lower crypt regions, which do not undergo RVD. Thus they are poor candidates for the NSP4 response.

Volume changes in response to Ca^{2+}-mediated secretagogues have been reported in CF mouse small intestinal crypts (56), suggesting that additional conductive pathways exist. The slow onset response observed for I^- influx after CCh challenge in $CFTR^{-/-}$ mouse crypts may reflect this alternate pathway (Fig. 6*B*). However, the timing of the effects of NSP4 in the $CFTR^{-/-}$ mouse crypt was very different (Fig. 7*B*), mimicking the profile observed for activation of apical membrane CFTR in wild-type crypts by all agonists (Figs. 5*A*, 6*A*, and 7*A*). We interpret these results to suggest that the effects of NSP4 on any basolateral membrane permeability, if present, are likely to be secondary phenomena and unrelated to the primary effects of NSP4 on the apical plasma membrane I^- influx.

A prosecretory model for NSP4-induced $[Ca^{2+}]_i$ mobilization. A characteristic property of rotavirus infection is that it causes age-dependent gastroenteritis in neonatal mammals (25). In the neonatal mouse, increases in small and large intestinal luminal Na^+, Cl^-, and water content have been correlated with diarrheal activity during rotaviral infection (49). Previously, we have reported (3) that NSP4 protein addition to mouse pup small intestinal mucosal sheets mimics the transepithelial Cl^- secretory effects of CCh, an endogenous Ca^{2+}-mobilizing agonist, but that this secretory response was lost in adult tissues. Further strengthening our hypothesis that enterocytes express an ontogenically regulated, Ca^{2+}-activated ionic conductance that underlies the diarrheal response, we now report that NSP4 induces Ca^{2+}-dependent, DIDS-inhibitable I^- influx in $CFTR^{-/-}$ mouse pup crypts. This phenomenon did not occur in adult crypts. The primary effect of NSP4 may therefore be to activate an apical plasma membrane Ca^{2+}-dependent Cl^- conductance in mouse pup enterocytes with biophysical properties similar to those described in vitro (19). The secondary effect of NSP4, like that of CCh, may be to facilitate CFTR-mediated fluid transport by upregulating Ca^{2+}-sensitive basolateral Cl^- uptake and cellular hyperpolarization. Combined, both may account for the Ca^{2+}-dependent fluid secretory response of normal and CF mucosa and may delineate a secretory component to rotaviral diarrhea.

An antiabsorptive model for NSP4-induced $[Ca^{2+}]_i$ mobilization. NSP4 mobilized Ca^{2+} in all regions of the crypt from both the small intestine and colon. We have also found that NSP4 is equally effective at mobilizing Ca^{2+} in dispersed villus epithelial cells from the small intestine (data not shown). Basal electroneutral NaCl absorption into the villus has been shown to be inhibited by Ca^{2+}-dependent processes, including PLC-γ, calmodulin, and protein kinase C activation (14, 17, 26). Thus another predicted secondary effect of NSP4-induced Ca^{2+} mobilization is downregulation of this absorptive process. Released NSP4 protein, if it encounters luminal receptors on neighboring cells (3), would be expected to promote similar antiabsorptive changes. NSP4-induced Ca^{2+} mobilization would not, however, be expected to affect absorptive Na^+-coupled glucose-solute transport (62), which is the cellular basis of oral rehydration therapy given during bacterial and viral gastroenteritis (40).

We have shown that the nonstructural protein of rotavirus NSP4 and its peptide both elevate intestinal cell $[Ca^{2+}]_i$ levels and induce diarrhea in neonatal mice with either wild-type or CFTR-deficient genotypes. Ca^{2+} mobilization may effect a diarrheal response in these cells through a variety of cellular mechanisms, including the activation of an ontogenically regulated, Ca^{2+}-sensitive, Cl^--conductive pathway in small intestinal crypts and Ca^{2+}-inhibitable Na^+-absorptive processes in small intestinal villi and crypts. Fluid loss by any of these mechanisms would occur independently of CFTR function. The diarrheal properties of NSP4 indicate that molecules based on the active domain of NSP4 may prove useful for the treatment of neonatal meconium ileus syndrome or the less severe clinical condition of constipation, which is prevalent in CF patients (44). The low dose (nanomolar) effectiveness of the NSP4 peptide and protein (3, 13), coupled with the fact that attenuated NSP4 proteins with differing diarrheal activities have been recently identified by us (64), suggests that further molecular characterization of the active domain of NSP4 may help design chemical structures with therapeutic value.

We thank Sharon Krater for help in breeding and genotyping the CF mice. We also thank A. Beaudet, F. Murad, R. O'Neal, and J. Sellin for critical evaluation of this manuscript.

This work was supported by National Institute of Diabetes and Digestive and Kidney Diseases Grant DK-30144 (M. K. Estes), Texas Advanced Technology Program Grant 004949–062 (M. K. Estes and A. P. Morris), and Cystic Fibrosis Foundation Postdoctoral Fellowship F806 (W. K. O'Neal).

Address for reprint requests and other correspondence: A. P. Morris, Depts. of Integrative Biology and Internal Medicine–Gastroenterology, Medical School, Univ. of Texas at Houston, Houston, TX 77030 (E-mail: amorris@girch1.med.uth.tmc.edu).

Received 1 February 1999; accepted in final form 12 May 1999.

REFERENCES

1. **Argons, G. A., W. R. Corse, R. I. Markowitz, E. S. Suarez, and D. R. Perry.** Gastrointestinal manifestations of cystic fibrosis: radiologic-pathologic correlation. *Radiographics* 16: 871–893, 1996.
2. **Angel, J., B. Tang, N. Feng, H. B. Greenberg, and D. Bass.** Studies of the role for NSP4 in the pathogenesis of homologous murine rotavirus diarrhea. *J. Infect. Dis.* 177: 455–458, 1998.
3. **Ball, J. M., P. Tian, C. Q. Zeng, A. P. Morris, and M. K. Estes.** Age-dependent diarrhea induced by a rotaviral nonstructural glycoprotein. *Science* 272: 101–104, 1996.
4. **Bateman, A., R. J. MacLeod, P. Lembessis, J. Hu, F. Esch, and S. Solomon.** The isolation and characterization of a novel corticostatin/defensin-like peptide from the kidney. *J. Biol. Chem.* 271: 10654–10659, 1996.
5. **Barnes, G. L.** Viral infections. In: *Pediatric Gastrointestinal Disease*, edited by A. W. Walker, P. R. Durie, J. R. Hamilton, J. A. Walker-Smith, and J. B. Watkins. St. Louis, MO: Mosby Year Book, 1996, chapt. 27, p. 654–663.
6. **Berschneider, H. M., M. R. Knowles, R. G. Azizkhan, R. C. Boucher, N. A. Tobey, R. C. Orlando, and D. W. Powell.** Altered intestinal chloride transport in cystic fibrosis. *FASEB J.* 2: 2625–2629, 1988.

7. **Chao, A. C., J. H. Widdicombe, and A. S. Verkman.** Chloride conductive and cotransport mechanisms in cultures of canine tracheal epithelial cells measured by an entrapped fluorescent indicator. *J. Membr. Biol*. 113: 193–202, 1990.
8. **Chiu, V. C., and D. H. Haynes.** High and low affinity Ca^{2+} binding to the sarcoplasmic reticulum: use of a high-affinity fluorescent calcium indicator. *Biophys. J*. 18: 3–22, 1977.
9. **De Clerck, L. S., C. H. Bridts, A. M. Mertens, M. M. Moens, and W. J. Stevens.** Use of fluorescent dyes in the determination of adherence of human leucocytes to endothelial cell and the effect of fluorochromes on cellular function. *J. Immunol. Methods* 172: 115–124, 1994.
10. **Desai, G. N., J. Sahi, P. M. Reddy, J. Venkatasubramanian, D. Vidyasagar, and M. C. Rao.** Chloride transport in primary cultures of rabbit colonocytes at different stages of development. *Gastroenterology* 111: 1541–1550, 1996.
11. **Diener, M.** Segmental differences along the crypt axis in the response of cell volume to secretagogues or hypotonic medium in the rat colon. *Pflügers Arch*. 426: 462–464, 1994.
12. **Diener, M., and V. Gartmann.** Effect of somatostatin on cell volume, Cl currents, and transepithelial Cl transport in rat distal colon. *Am. J. Physiol*. 266 (*Gastrointest. Liver Physiol*. 29): G1043–G1052, 1994.
13. **Dong, Y., C. Q. Zeng, J. M. Ball, M. K. Estes, and A. P. Morris.** The rotavirus enterotoxin NSP4 mobilizes intracellular calcium in human intestinal cells by stimulating phospholipase C-mediated inositol 1,4,5-trisphosphate production. *Proc. Natl. Acad. Sci. USA* 412: 3960–3965, 1997.
14. **Donowitz, M., M. E. Cohen, M. Gould, and G. W. G. Sharp.** Elevated intracellular Ca^{2+} acts through protein kinase C to regulate rabbit ileal NaCl absorption. *J. Clin. Invest*. 83: 1953–1962, 1989.
15. **Dorin, J. R.** Development of mouse models for cystic fibrosis. *J. Inherit. Metab. Dis*. 18: 495–500, 1995.
16. **Dubois-Dalcq, M., K. V. Holmes, and B. Rentier.** Assembly of rotaviruses. In: *Assembly of Enveloped RNA Viruses*, edited by D. W. Kingsbury. New York: Springer-Verlag, 1986, chapt. 10, p. 171–182.
17. **Emmer, E., R. P. Rood, J. H. Wesolek, M. E. Cohen, R. S. Braithwaite, G. W. G. Sharp, H. Murer, and M. Donowitz.** Role of calcium and calmodulin in the regulation of the rabbit ileal brush-border membrane Na^+/H^+ antiporter. *J. Membr. Biol*. 108: 207–215, 1989.
18. **Estes, M. K., E. L. Palmer, and J. F. Obijeski.** Rotaviruses: a review. *Curr. Top. Microbiol. Immunol*. 105: 123–184, 1983.
19. **Frizzel, R. A., and A. P. Morris.** Chloride conductances of salt-secreting epithelial cells. In: *Current Topics in Membranes—Chloride Channels*, edited by W. B. Guggino. San Diego, CA: Academic, 1994, chapt. 6, p. 173–214, 1994.
20. **Goldstein, J. L., J. Sahi, M. Bhuva, T. J. Layden, and M. C. Rao.** *Escherichia coli* heat-stable enterotoxin-mediated colonic Cl^- secretion is absent in cystic fibrosis. *Gastroenterology* 107: 950–956, 1994.
21. **Grynkiewicz, G., M. Poenie, and R. Y. Tsien.** A new generation of Ca^{2+} indicators with greatly improved fluorescence properties. *J. Biol. Chem*. 260: 3440–3450, 1985.
22. **Halm, D. R., K. L. Kirk, and K. C. Sathiakumar.** Stimulation of Cl permeability in colonic crypts of Lieberkuhn measured with a fluorescent indicator. *Am. J. Physiol*. 265 (*Gastrointest. Liver Physiol*. 28): G423–G431, 1993.
23. **Hasty, P., W. K. O'Neal, K. Q. Liu, A. P. Morris, Z. Bebok, G. B. Shumyatsky, T. Jilling, E. J. Sorscher, A. Bradley, and A. L. Beaudet.** Severe phenotype in mice with termination mutation in exon 2 of cystic fibrosis gene. *Somat. Cell Mol. Genet*. 21: 177–187, 1995.
24. **Illsley, N. P., and A. S. Verkman.** Membrane chloride transport measured using a chloride-sensitive fluorescent probe. *Biochemistry* 26: 1215–1219, 1987.
25. **Kapikian, A. Z., and R. M. Chanock.** Rotaviruses. In: *Virology*, edited by B. N. Fields, D. M. Knipe, and P. M. Howley. New York: Raven, 1996, chapt. 55, p. 1657–1708.
26. **Khurana, S., S. Kreydiyyeh, A. Aronzon, W. A. Hoogerwerf, S. G. Rhee, M. Donowitz, and M. E. Cohen.** Asymmetric signal transduction in polarized ileal $Na(^+)$absorbing cells: carbachol activates brush-border but not basolateral-membrane PIP2-PLC and translocates PLCγ 1 only to the brush border. *Biochem. J*. 313: 509–518, 1996.
27. **Krapf, R., N. P. Illsley, H. C. Tseng, and A. S. Verkman.** Structure-activity relationships of chloride-sensitive fluorescent indicators for biological application. *Anal. Biochem*. 169: 142–150, 1988.
28. **Lakowicz, J. R.** Quenching of fluorescence. In: *Principles of Fluorescence Spectroscopy*. New York: Plenum, 1983, chapt. 9, p. 257–289.
29. **Leipziger, J., D. Kerstan, R. Nitschke, and R. Greger.** ATP increases $[Ca^{2+}]_i$ and ion secretion via a basolateral P2Y-receptor in rat distal colonic mucosa. *Pflügers Arch*. 434: 77–83, 1997.
30. **Lencer, W. I., G. Cheung, G. R. Strohmeier, M. G. Currie, A. J. Ouellette, M. E. Selsted, and J. L. Madara.** Induction of epithelial chloride secretion by channel-forming cryptdins 2 and 3. *Proc. Natl. Acad. Sci. USA* 94: 8585–8589, 1997.
31. **MacLeod, R. J., J. R. Hamilton, A. Bateman, D. Belcourt, J. Hu, H. P. Bennett, and S. Solomon.** Corticostatic peptides cause nifedipine-sensitive volume reduction in jejunal villus enterocytes. *Proc. Natl. Acad. Sci. USA* 88: 552–556, 1991.
32. **Mathews, D. E., and V. T. Farewell.** Fisher test for 2×2 contingency tables. In: *Using and Understanding Medical Statistics* (3rd ed.). New York: Karger, 1996, chapt. 3, p. 19–37.
33. **Michelangeli, F., F. Liprandi, M. E. Chemello, M. Ciarlet, and M. C. Ruiz.** Selective depletion of stored calcium by thapsigargin blocks rotavirus maturation but not the cytopathic effect. *J. Virol*. 69: 3838–3847, 1995.
34. **Michelangeli, F., M. C. Ruiz, J. R. del Castillo, J. E. Ludert, and F. Liprandi.** Effect of rotavirus infection on intracellular calcium homeostasis in cultured cells. *Virology* 181: 520–527, 1991.
35. **Morris, A. P., K. L. Kirk, and R. A. Frizzell.** Simultaneous analysis of cell Ca^{2+} and Ca^{2+}-stimulated chloride conductance in colonic epithelial cells. *Cell Regul*. 1: 951–963, 1990.
36. **O'Grady, S. M., H. C. Palfrey, and M. Field.** Characteristics and functions of Na-K-Cl cotransport in epithelial tissues. *Am. J. Physiol*. 253 (*Cell Physiol*. 22): C177–C192, 1987.
37. **O'Loughlin, E. V., D. M. Hunt, K. J. Gaskin, D. Stiel, I. M. Bruzuszcak, H. C. Martin, C. Bambach, and R. Smith.** Abnormal epithelial transport in cystic fibrosis jejunum. *Am. J. Physiol*. 260 (*Gastrointest. Liver Physiol*. 23): G758–G763, 1991.
38. **Osborne, M. P., S. J. Haddon, A. J. Spencer, J. Collins, W. G. Starkey, T. S. Wallis, G. J. Clarke, K. J. Worton, D. C. Candy, and J. Stephen.** An electron microscopic investigation of time-related changes in the intestine of neonatal mice infected with murine rotavirus. *J. Pediatr. Gastroenterol. Nutr*. 7: 236–248, 1988.
39. **Poruchynsky, M. S., D. R. Maass, and P. H. Atkinson.** Calcium depletion blocks the maturation of rotavirus by altering the oligomerization of virus-encoded proteins in the ER. *J. Cell Biol*. 114: 651–656, 1991.
40. **Rabalais, G. P.** Recent advances in the prevention and treatment of diarrheal diseases. *Curr. Opin. Infect. Dis*. 9: 210–213, 1996.
41. **Ram, S. J., and K. L. Kirk.** Cl^- permeability of human sweat duct cells monitored with fluorescence-digital imaging microscopy: evidence for reduced plasma membrane Cl^- permeability in cystic fibrosis. *Proc. Natl. Acad. Sci. USA* 86: 10166–10170, 1989.
42. **Rich, D. P., M. P. Anderson, R. J. Gregory, S. H. Cheng, S. Paul, D. M. Jefferson, J. D. McCann, K. W. Klinger, A. E. Smith, and M. J. Welsh.** Expression of cystic fibrosis transmembrane conductance regulator corrects defective chloride channel regulation in cystic fibrosis airway epithelial cells. *Nature* 347: 358–363, 1990.
43. **Riordan, J. R., J. M. Rommens, B. S. Kerem, N. Alon, R. Rozmahel, Z. Grzelczak, J. Zielenski, S. Lok, N. Plavsic, J.-L. Chou, M. L. Drumm, M. C. Iannuzzi, F. S. Collins, and L.-C. Tsui.** Identification of the cystic fibrosis gene: cloning and characterization of complementary DNA. *Science* 245: 1066–1073, 1989.
44. **Rubenstein, S., R. Moss, and N. Lewiston.** Constipation and meconium ileus equivalent in patients with cystic fibrosis. *Pediatrics* 78: 473–479, 1986.

45. **Sahi, J., J. L. Goldstein, T. J. Layden, and M. C. Rao.** Cyclic AMP- and phorbol ester-regulated Cl^- permeabilities in primary cultures of human and rabbit colonocytes. *Am. J. Physiol.* 266 (*Gastrointest. Liver Physiol.* 29): G846–G855, 1994.
46. **Sahi, J., M. P. Wiggins, G. B. Gibori, T. J. Layden, and M. C. Rao.** Calcium regulated chloride permeabilities in primary cultures of rabbit colonocytes. *J. Cell. Physiol.* 168: 276–283, 1996.
47. **Satoh, Y., Y. Habara, K. Ono, and T. Kanno.** Carbamylcholine- and catecholamine-induced intracellular calcium dynamics of epithelial cells in mouse ileal crypts. *Gastroenterology* 108: 1345–1356, 1995.
48. **Shalon, L. B., and J. W. Adelson.** Cystic fibrosis. Gastrointestinal complications and gene therapy. *Pediatr. Clin. North Am.* 43: 157–196, 1996.
49. **Starkey, W. G., J. Collins, D. C. A. Candy, A. J. Spencer, M. P. Osborne, and J. Stephen.** Transport of water and electrolytes by rotavirus-infected mouse intestine: a time course study. *J. Pediatr. Gastroenterol. Nutr.* 11: 254–260, 1990.
50. **Stern, M., F. M. Munkonge, N. J. Caplen, F. Sorgi, L. Huang, D. M. Geddes, and E. W. Alton.** Quantitative fluorescence measurements of chloride secretion in native airway epithelium from CF and non-CF subjects. *Gene Ther.* 2: 766–774, 1995.
51. **Strabel, D., and M. Diener.** Evidence against direct activation of chloride secretion by carbachol in the rat distal colon. *Eur. J. Pharmacol.* 274: 181–191, 1995.
52. **Stutzin, A., A. L. Eguiguren, L. P. Cid, and F. V. Sepulveda.** Modulation by extracellular Cl^- of volume-activated organic osmolyte and halide permeabilities in HeLa cells. *Am. J. Physiol.* 273 (*Cell Physiol.* 42): C999–C1007, 1997.
53. **Taylor, C. J., P. S. Baxter, J. Hardcastle, and P. T. Hardcastle.** Failure to induce secretion in jejunal biopsies from children with cystic fibrosis. *Gut* 29: 957–962, 1988.
54. **Tsui, L. C.** The cystic fibrosis transmembrane conductance regulator gene. *Am. J. Respir. Crit. Care Med.* 151: S47–S53, 1995.
55. **Valverde, M. A., J. A. O'Brien, F. V. Sepulveda, R. A. Ratcliff, M. J. Evans, and W. H. Colledge.** Impaired cell volume regulation in intestinal crypt epithelia of cystic fibrosis mice. *Proc. Natl. Acad. Sci. USA* 92: 9038–9041, 1995.
56. **Valverde, M. A., J. A. O'Brien, F. V. Sepulveda, R. Ratcliff, M. J. Evans, and W. H. Colledge.** Inactivation of the murine cftr gene abolishes cAMP-mediated but not $Ca(^{2+})$ mediated secretagogue-induced volume decrease in small-intestinal crypts. *Pflügers Arch.* 425: 434–438, 1993.
57. **Vellenga, L., H. J. Egberts, T. Wensing, J. E. van Dijk, J. M. V. M. Mouwen, and H. J. Breukink.** Intestinal permeability in pigs during rotavirus infection. *Am. J. Vet. Res.* 53: 1180–1183, 1992.
58. **Verkman, A. S.** Development and biological applications of chloride-sensitive fluorescent indicators. *Am. J. Physiol.* 259 (*Cell Physiol.* 28): C375–C388, 1990.
59. **Verkman, A. S., A. C. Chao, and T. Hartmann.** Hormonal regulation of Cl transport in polar airway epithelia measured by a fluorescent indicator. *Am. J. Physiol.* 262 (*Cell Physiol.* 31): C23–C31, 1992.
60. **Welsh, M. J.** Cystic fibrosis. In: *Molecular Biology of Membrane Transport Disorders*, edited by S. G. Schultz, T. E. Andreoli, A. M. Brown, D. M. Fambrough, J. F. Hoffman, and M. J. Welsh. New York: Plenum, 1996, p. 605–619.
61. **Woll, E., M. Gschwentner, J. Furst, S. Hofer, G. Buemberger, A. Jungwirth, J. Frick, P. Deetjen, and M. Paulmichl.** Fluorescence-optical measurements of chloride movements in cells using the membrane-permeable dye diH-MEQ. *Pflügers Arch.* 432: 486–493, 1996.
62. **Wright, E. M.** The intestinal Na^+/glucose cotransporter. *Annu. Rev. Physiol.* 55: 575–589, 1993.
63. **Yao, B., D. L. Hogan, K. Bukhave, M. A. Koss, and J. I. Isenberg.** Bicarbonate transport by rabbit duodenum in vitro: effect of vasoactive intestinal polypeptide, prostaglandin E2, and cyclic adenosine monophosphate. *Gastroenterology* 104: 732–740, 1993.
64. **Zhang, M., C. Q.-Y. Zeng, Y. Dong, J. M. Ball, L. J. Saif, A. P. Morris, and M. K. Estes.** Mutations in rotavirus nonstructural glycoprotein NSP4 are associated with altered virus virulence. *J. Virol.* 72: 3666–3672, 1997.